JOURNAL OF GEOPHYSICAL RESEARCH, VOL. 117, A05306, doi:10.1029/2011JA017232, 2012

Large-scale observations of a subauroral polarization stream by midlatitude SuperDARN radars: Instantaneous longitudinal velocity variations

L. B. N. Clausen,[1,2] J. B. H. Baker,[1] J. M. Ruohoniemi,[1] R. A. Greenwald,[1] E. G. Thomas,[1] S. G. Shepherd,[3] E. R. Talaat,[4] W. A. Bristow,[5] Y. Zheng,[6] A. J. Coster,[7] and S. Sazykin[8]

Received 5 October 2011; revised 19 March 2012; accepted 21 March 2012; published 4 May 2012.

[1] We present simultaneous measurements of flow velocities inside a subauroral polarization stream (SAPS) made by six midlatitude high-frequency SuperDARN radars. The instantaneous observations cover three hours of universal time and six hours of magnetic local time (MLT). From velocity variations across the field-of-view of the radars we infer the local 2D flow direction at three different longitudes. We find that the local flow direction inside the SAPS channel is remarkably constant over the course of the event. The flow speed, however, shows significant temporal and spatial variations. After correcting for the radar look direction we are able to accurately determine the dependence of the SAPS velocity on magnetic local time. We find that the SAPS velocity variation with magnetic local time is best described by an exponential function. The average velocity at 00 MLT was 1.2 km/s and it decreased with a spatial e-folding scale of two hours of MLT toward the dawn sector. We speculate that the longitudinal distribution of pressure gradients in the ring current is responsible for this dependence and find these observations in good agreement with results from ring current models. Using TEC measurements we find that the high westward velocities of the SAPS are - as expected - located in a region of low TEC values, indicating low ionospheric conductivities.

Citation: Clausen, L. B. N., et al. (2012), Large-scale observations of a subauroral polarization stream by midlatitude SuperDARN radars: Instantaneous longitudinal velocity variations, *J. Geophys. Res.*, *117*, A05306, doi:10.1029/2011JA017232.

1. Introduction

[2] Strong westward flows in the subauroral ionosphere were first reported in low-altitude satellite data by *Galperin et al.* [1973] and independently by *Spiro et al.* [1979]. The drifts are caused by strong electric fields oriented northward in the ionosphere which were first studied by *Smiddy et al.* [1977]. *Yeh et al.* [1991] used incoherent scatter radar data to characterize a number of such enhanced westward flows, albeit these events had a larger latitudinal extent than those previously reported. A number of terms have been used to describe these related phenomena, such as polarization jet (PJ) [*Galperin*, 2002] or subauroral ion drift (SAID) [*Anderson et al.*, 2001]. *Foster and Burke* [2002] suggested that all these events be described by the inclusive term subauroral polarization stream (SAPS). A SAPS is then defined as a relatively narrow channel (~5° magnetic latitude) of enhanced westward flow, located just equatorward of the lower auroral electron precipitation boundary on the nightside. Embedded within this relatively broad channel of westward flows one sometimes observes a second, narrower (~1° magnetic latitude) channel of even higher (several km/s) westward flows; this localized feature is commonly referred to as a SAID.

[3] Using velocity data from the Millstone Hill incoherent scatter radar spanning two complete solar cycles, *Foster and Vo* [2002] presented a comprehensive statistical study of SAPS. They show that the position, extent, and intensity of the SAPS varies with geomagnetic activity. In the pre-midnight sector, SAPS on average span 2–3° magnetic latitude, occur at magnetic latitudes of ~60°, and have an average

[1]Bradley Department of Electrical and Computer Engineering, Virginia Polytechnic Institute and State University, Blacksburg, Virginia, USA.
[2]Now at Institute for Geophysics and Extraterrestrial Physics, Technische Universität Braunschweig, Braunschweig, Germany.
[3]Thayer School of Engineering, Dartmouth College, Hanover, New Hampshire, USA.
[4]Johns Hopkins University Applied Physics Laboratory, Laurel, Maryland, USA.
[5]Geophysical Institute, University of Alaska Fairbanks, Fairbanks, Alaska, USA.
[6]NASA Goddard Space Flight Center, Greenbelt, Maryland, USA.
[7]Haystack Observatory, Massachusetts Institute of Technology, Westford, Massachusetts, USA.
[8]Department of Physics and Astronomy, Rice University, Houston, Texas, USA.

Corresponding Author: L. B. N. Clausen, Institute for Geophysics and Extraterrestrial Physics, Technische Universität Braunschweig, Braunschweig D-38106, Germany. (l.clausen@tu-braunschweig.de)

0148-0227/12/2011JA017232

velocity of 1000 m/s. Post-midnight the average velocity decreases to about 400 m/s, as does the occurrence latitude, whereas the latitudinal extent increases slightly. Below Kp values of 5 the velocity within the SAPS channel seems to decrease linearly with magnetic local time.

[4] Later, *Erickson et al.* [2011] used the same dataset to study in detail the statistical dependence of convective ion flux and velocity of SAPS on MLT and geomagnetic activity. They show that SAPS account for significant bulk mass flux of oxygen ions in the ionosphere toward the noontime cusp. This highlights the important role SAPS play in understanding the intricacies of magnetosphere-ionosphere coupling. Furthermore, independent of geomagnetic activity as characterized by Dst index, they also find that statistically the peak ion westward velocity inside SAPS varies linearly with MLT on the nightside between 14 and 05 MLT.

[5] These large statistical studies show that SAPS tend to occur during magnetically disturbed periods when a duskward electric field drives both plasma sheet ions and electrons from the distant magnetotail earthward via $\vec{E} \times \vec{B}$ drift. As the particles approach Earth, they begin to feel the effect of the corotational electric field [*Kavanagh et al.*, 1968] and are also experiencing forces due to magnetic curvature and gradients. Consequently, the ions start drifting westward and the electrons drift eastward around Earth. Another important consequence of these drift paths is the formation of an Alfvén layer [*Alfvén*, 1955, 1958] which separates the open drift paths connecting the tail to the magnetopause from closed drift paths on which particles orbit around Earth. At these boundaries pitch angle scattering causes ion and electron precipitation into the subauroral ionosphere [*Kennel*, 1969; *Southwood and Wolf*, 1978].

[6] Different energy spectra of the ion and electron distribution can cause a misalignment between the locations of the ion and electron Alfvén layers and hence large polarization electric fields can form between them. As magnetic field lines can be considered good conductors and hence electrostatic equipotentials, these potential drops also apply at the footprint of the involved magnetic flux tubes in the ionosphere. Radial electric fields in the magnetospheric equatorial plane then translate to north-south aligned electric fields in the ionosphere. Considering the orientation of the background magnetic field in the northern hemisphere, northward electric fields will drive the observed westward flows inside the SAPS, if the ion Alfvén layer is located earthward of the electron boundary [*Wolf et al.*, 2007].

[7] One shortcoming of the above theory is the obvious omission of field-aligned currents (FACs). To rectify this, *Anderson* [1993] proposed that the separation of the precipitation boundaries in the magnetospheric equatorial plane does not cause the strong electric fields associated with SAPS. Instead, misalignment between the ion and electron precipitation boundaries causes a separation of the location of FACs which are driven by precipitating ions and electrons. These FACs dump charged particles in the subauroral ionosphere. If the particles are dumped in a region of low conductance, such as the ionospheric density trough, only a small closure current will flow between the separated footprints of the FACs, allowing a large polarization electric field to build up. In fact, large electric fields in the ionosphere cause a decrease in conductivity [*Schunk et al.*, 1976; *Banks and Yasuhara*, 1978] which leads to a positive feedback mechanism, allowing the electric fields to grow even larger and hence causing higher drift velocities inside the SAPS.

[8] The plasma sheet particles that are responsible for the polarization electric fields that cause SAPS also form the ring current. It is well known that pressure gradients inside the ring current drive FACs, such that the distribution of the ring current plasma pressure with radial distance from Earth and MLT can be expected to influence the drift velocities of SAPS observed in the subauroral ionosphere. By now quite sophisticated and well-tested models of the ring current and its parameters exist, such as the Rice Convection Model [e.g., *Toffoletto et al.*, 2003], such that the behavior of the ring current during disturbed periods is quite well understood. Furthermore, *Zheng et al.* [2008] coupled a ring current model to an ionospheric conductivity model and were able to predict the large-scale behavior of the velocity inside the SAPS in the subauroral ionosphere.

[9] Until recently, simultaneous measurements of velocities inside the SAPS were available at a limited number of different magnetic local times only, either from one or several polar orbiting satellites crossing the flow channel or from incoherent scatter radar measurements along some look direction. Slightly larger longitudinal extents of the velocity distribution were presented in SAPS studies using single SuperDARN radars [*Oksavik et al.*, 2006; *Makarevich et al.*, 2009]. Although both *Foster and Vo* [2002] and *Erickson et al.* [2011] show the MLT dependence of drift velocities inside the SAPS channel, these are always averages of many disconnected events, rather than instantaneous measurements. In this paper we present, for the first time, large-scale simultaneous observations of the longitudinal velocity structure of SAPS using data from the new midlatitude chain of SuperDARN radars.

1.1. SuperDARN Radars at Midlatitudes

[10] SuperDARN is a network of radars operating in the high-frequency band, typically between 8 and 18 MHz [*Greenwald et al.*, 1995; *Chisham et al.*, 2007]. These radars are capable of electronically steering their look direction; each look direction is called a beam. The number of beams available varies for different radars, however each beam is typically around 3° wide such that the field-of-view (FOV) of a radar with 16 beams covers about 50°. As of September 2011, 18 radars operate in the northern hemisphere. In Figure 1 we show, in magnetic coordinates, the FOVs of these radars. Orange coloring is used for radars located at midlatitudes, high-latitude radars are colored gray and the FOVs of the two radars looking into the polar cap have been colored blue.

[11] SuperDARN radars record the signal backscattered from decameter density structures in the ionosphere which are aligned with the background magnetic field. These density irregularities typically occur in the F-region where they $\vec{E} \times \vec{B}$ drift with the background plasma [*Ruohoniemi et al.*, 1987]. In standard mode the analysis of the backscattered signal yields backscattered power (signal-to-noise ratio), the line-of-sight (LOS) component of the density irregularity drift velocity and the spectral width of the irregularities in 75 to 100 sections along each beam; these sections are called

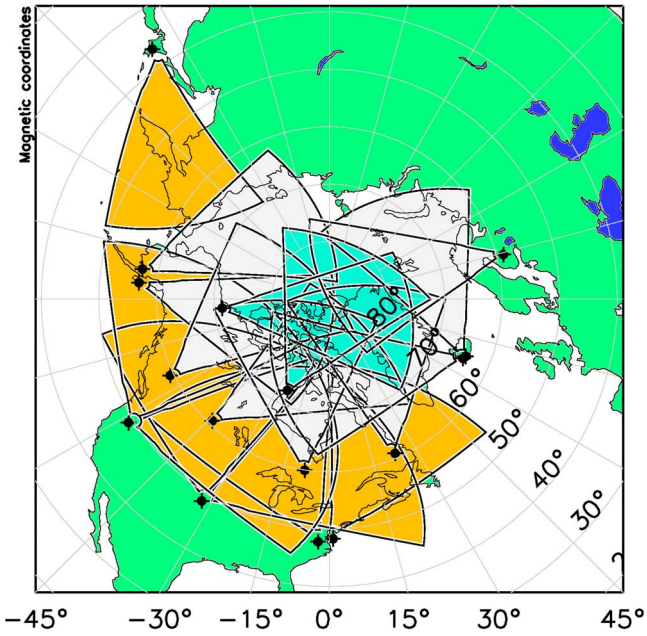

Figure 1. Fields-of-view of the SuperDARN radars located in the northern hemisphere in magnetic coordinates as of September 2011. Radars located at 70° are colored blue, those located at 60° are shown in gray and the midlatitude radars at 50° are colored orange.

range gates and are each 45 km long. The look direction - or azimuth - of a beam is measured in degree relative to magnetic North and will in this study be called α.

[12] This work was made possible by the ongoing development of a midlatitude chain of SuperDARN HF radars. Traditionally located around magnetic latitudes of $\Lambda = 60°$ and looking into the auroral zone and the polar cap, the SuperDARN network expanded in the southern hemisphere into the midlatitude region at the end of 1999, when a radar was erected on the southern tip of Tasmania ($\Lambda = -54.8°$). In 2005, the first SuperDARN radar at midlatitudes in the northern hemisphere was constructed at Wallops Island, Virginia ($\Lambda = 48.3°$). This was followed by the deployment of radars on Hokkaido, Japan in 2007 and at Blackstone, Virginia in 2008. Beginning in 2009, the NSF funded the construction of eight additional radars distributed over four sites under the Mid-Sized Infrastructure (MSI) program. The new radars are meant to combine with the existing midlatitude radars to make an unbroken chain of coverage that extends from the west coast of Europe through the North American sector to the east coast of Asia, their FOVs covering over ten hours of local time. The midlatitude chain complements the existing high-latitude chain. To the extent possible, the MSI radars are oriented in pairs to make possible common-volume observations. The first MSI radar facility was built at Hays, Kansas in 2009 and the second was built at Christmas Valley, Oregon in 2010. Further builds are scheduled for the Aleutians and for the Azores. The collaborating institutions on the MSI project are Virginia Tech, Dartmouth College, University of Alaska Fairbanks, and the Johns Hopkins University Applied Physics Laboratory. As of May 2011, six radars located below $\Lambda = 50°$ span the midlatitude region over the North American sector. Their names, abbreviations, geomagnetic locations, boresites with respect to geographic North, number of beams and the date when operations began are given in Table 1.

2. Observations

[13] On 09 April 2010 between 0700 and 1000 UT all six midlatitude SuperDARN radars located in northern America observed enhanced westward flows with FOVs covering more than six hours of magnetic local time. In Figure 2 we show LOS velocities measured by the Christmas Valley West (CVW) and Christmas Valley East (CVE) radars at 0840 UT, in magnetic coordinates [*Baker and Wing*, 1989]. At this time, the radars were located around magnetic midnight; the 00 MLT meridian is indicated by a dashed line. The measured velocities are colored-coded according to the color bar on the right; note the non-linear scaling. In the SuperDARN convention, movement away from the radar corresponds to negative velocities (colored red), velocities associated with movement toward the radar are positive (colored blue).

[14] Four regions of radar backscatter were observed at 0840 UT by the radars located in Oregon, each is marked by Roman numerals in Figure 2. Low velocity backscatter - type *I* - was measured at very close range gates, colored in green; this scatter type is typically associated with meteor trails that drift with neutral wind velocities in the D-region of the ionosphere at about 90 km altitude [*Hall et al.*, 1997]. Located just above 50° magnetic latitude west of the radar location and marked as type *II*, a patch associated with velocities around −100 m/s was observed. These are most likely part of the low-velocity subauroral scatter that is commonly observed by the midlatitude SuperDARN radars [*Greenwald et al.*, 2006]. It is moving away from the radar, i.e. westward, as is often the case [*Ribeiro et al.*, 2011]. Located around 60° magnetic latitude a band of high velocities was observed, covering about four hours of local time (type *III*). This channel was ∼3° of magnetic latitude

Table 1. Information About the Six SuperDARN Radars Located at Midlatitudes in Northern America

Name	Abbreviation	Magnetic Latitude (deg)	Magnetic Longitude (deg)	Bore Site (deg)	Number of Beams	Date Operational Since
Wallops Island, VA	WAL	48.3	+0.9	+36	16	Jun. 2005
Blackstone, VA	BKS	47.8	−2.6	−32	16	Feb. 2008
Fort Hays East, KS	FHE	48.5	−32.3	+45	22	Feb. 2010
Fort Hays West, KS	FHW	48.5	−32.3	−25	22	Feb. 2010
Christmas Valley East, OR	CVE	49.1	−58.4	+54	24	Jan. 2011
Christmas Valley West, OR	CVW	49.1	−58.4	−20	24	Jan. 2011

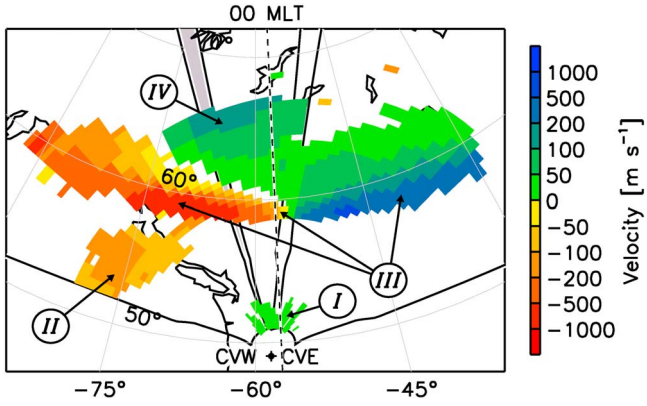

Figure 2. Line-of-sight velocities observed on 09 April 2011 at 0840 UT by the Christmas Valley radar pair located in Oregon, USA, plotted in magnetic coordinates. The 00 MLT meridian is shown as a dashed line. Beam 16 of the Christmas Valley West radar is highlighted by the gray shading. Four regions of radar backscatter are marked by capital Roman numerals (see text for details).

wide. Figure 2 clearly shows how the LOS velocities within this band vary as a function of beam, from ionospheric drift toward the radar in the eastern FOV to motion away from the radar in the west; this then indicates that the flow was directed westward. The most intense velocities were observed just before local midnight, where the drift exceeded 1000 m/s. Poleward of this channel of high-velocity scatter, the radars observed a region of moderate velocities >100 m/s (type *IV*). This region is in the western parts of the FOVs separated in latitude from the high-velocity channel. It is located at magnetic latitudes above 62° around 00 MLT, directed toward the radars and hence most probably a signature of the anti-sunward plasma flow across the polar cap as part of the two-cell convection that occurs at high-latitudes [*Ruohoniemi and Greenwald*, 1996].

[15] To relate the occurrence of the SAPS to the magnetospheric state, we show in Figure 3 solar wind and magnetospheric activity parameters over a three day period between 08 April 2011 (doy 98) and 10 April 2011 (doy 100). The first, second, and third panels show the solar wind speed, total interplanetary magnetic field (IMF), and the IMF Bz component from the OMNI database [*King and Papitashvili*, 2006]. In the fourth, fifth, and sixth panels we show some magnetospheric parameters: the Kp index as an indicator for global geomagnetic activity, followed by the AU (dotted line) and AL (solid line) indices which are measures of auroral activity, and, in the sixth panel of Figure 3, the Sym-H (solid line) and Asym-H (dotted line) indices that provide information about the strength of the symmetric and asymmetric part of the ring current, respectively. The interval during which high westward flows were observed by the SuperDARN radars is marked by vertical dashed lines. Figure 3 then shows that the event occurred during a period of decreasing Kp index; 9 hours before the observation of the event the Kp index was 4 and subsequently decreased to reach a value of 2 at the time of the event. The enhancement in magnetospheric activity was due to a southward turning of the IMF Bz component during the second half of doy 98 (08 April 2011). During the event discussed in this paper the ring current was enhanced (Sym-H $\sim$ −50nT), and a moderate auroral activation concurrent with an increase in the asymmetric ring current was observed.

[16] In Figure 4 we show a range-time plot of the line-of-sight velocity measured by the Christmas Valley West radar along beam 16 between 0400 and 1000 UT on 09 April 2011. This beam is also marked in gray in Figure 2. The velocities are plotted against magnetic latitude Λ on the y axis; they are color-coded according to the color bar to the top of the panel. At 60° magnetic latitude beam 16 of the CVW radar is aligned at an angle of about −18° relative to magnetic North; negative angles indicate anti-clockwise rotation. Hence negative velocities, i.e. movement away from the radar, along beam 16 are consistent with a westward/poleward sense of flow, while positive velocities are indicative for equatorward or eastward flows. It can be seen from the first panel of Figure 4 that at higher latitudes the observed flows after 0630 UT were predominantly positive (colored green to blue), i.e. directed toward the radar. Considering the location of the radar around 00 MLT, this is consistent with anti-sunward flow across the polar cap as part of the two-cell convection that is often observed. Toward lower latitudes a narrow channel of highly negative - westward - velocities was observed. For each sounding along beam 16 we have marked the maximum negative, i.e. westward, velocity with a black dot. These maximum velocities have

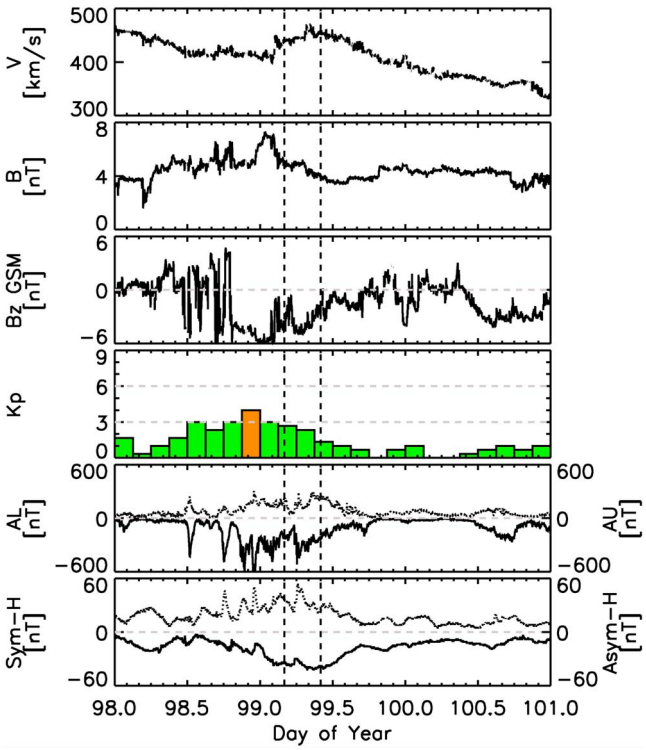

Figure 3. Time series stackplot of the solar wind velocity, total interplanetary magnetic field (IMF), the IMF Bz component, the Kp index, the AL (solid line) and AU (dashed line) index followed by the Sym-H (solid line) and the Asym-H (dotted line) index. The time of enhanced westward flows observed by the SuperDARN radars is marked by vertical dashed lines.

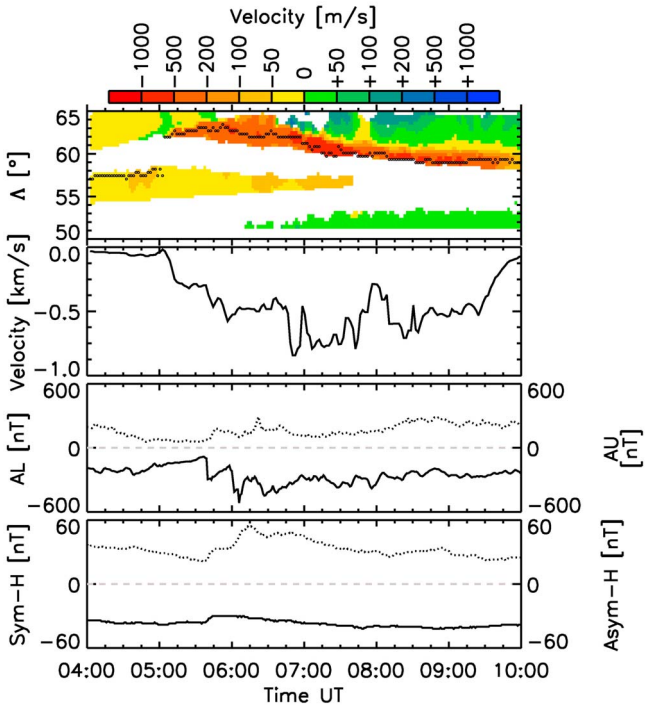

Figure 4. The first panel shows the LOS velocities measured by the CVW radar along beam 16 against magnetic latitude Λ (compare Figure 2). At each time step the maximum negative velocity is marked by a black dot. For this radar and this beam negative velocities are consistent with a westward sense of the flow. The second panel shows these maximum westward velocities, followed by the AL (solid line) and AU (dotted line) index (third panel), and the Sym-H (solid line) and Asym-H (dotted line) index in the fourth panel.

also been plotted in the second panel. The third and fourth panels again show the AU, AL, Sym-H and Asym-H indices in the same format as in Figure 3. The maximum westward velocities show considerable temporal variations throughout the event; a correlation between the activity indices and the velocity variations is not obvious from Figure 4. This lack of correlation is not surprising as the four magnetic activity indices are derived from global magnetometer data whereas the velocity data were measured in a comparatively small volume.

[17] Figure 5 gives an overview of the measurements at 0840 UT from all midlatitude radars in North America, and compared with GPS TEC measurements and electron precipitation from the NOAA POES satellites [*Evans and Greer*, 2000]. Figure 5 (top) shows a map of median-filtered TEC measurements [*Rideout and Coster*, 2006; *Coster et al.*, 2007] in magnetic coordinates and the location of velocity measurements made by the radars as small black dots. The downward electron flux measured by the POES-18 satellite are overlaid as colored dots. Figure 5 (bottom) shows, again in magnetic coordinates, the velocity measurements by the radars colored according to the color bar on the right. In both panels we show a model auroral oval representation following *Holzworth and Meng* [1975] for a Kp index of 2 (compare Figure 3) and the location of the 00 MLT meridian as a dashed line.

[18] In Figure 5 (top) a distinct region of low TEC was observed below 60° magnetic latitude at 00 MLT and at lower latitudes toward the dusk flank of the magnetosphere, ranging to latitudes as low as 50°. We interpret these low TEC values as the signature of the density trough. This region of the ionosphere is characterized by low electron densities, making it a poor conductor. Figure 5 (top) also shows that the bulk of the observations of the high-velocity flows were made along the poleward edge of the ionospheric footprint of the density trough.

[19] Figure 5 (bottom) shows that all midlatitude radars observed a relatively narrow (∼3° of magnetic latitude) channel of enhanced flow. It can be seen from Figure 5 that throughout the FOVs of those radars looking to the East (CVE, FHE, and WAL), the flow within the channel is toward the radar, colored green to blue. In the FOVs of the radars looking to the West (CVW, FHW, and BKS), the flow is directed away from the radar (negative, colored yellow to red). This then shows that the flow of the SAPS is predominantly westward. The observed velocities inside the channel are much higher over the western parts of the

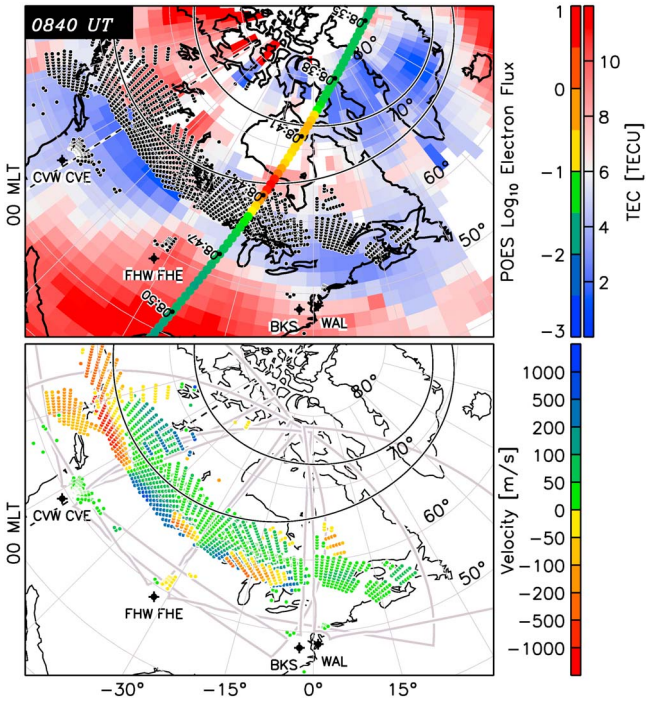

Figure 5. Overview of the measurements made of the SAPS channel by all six midlatitude radars on 09 April 2011, 0840 UT in magnetic coordinates. (top) Median-filtered GPS TEC measurements colored blue to red. The large colored dots show the down-going electron flux measured by the POES-18 satellite along its track, the times of the measurements are given next to the track. The small black dots give the locations of velocity measurements made by the six radars. (bottom) The measured velocities, now color-coded according to the color bar on the right; note the non-linear scaling. We also show the radar FOVs as gray lines. In both panels we show the auroral oval for a Kp index of 2 following *Holzworth and Meng* [1975] and mark the 00 MLT meridian by a dashed line.

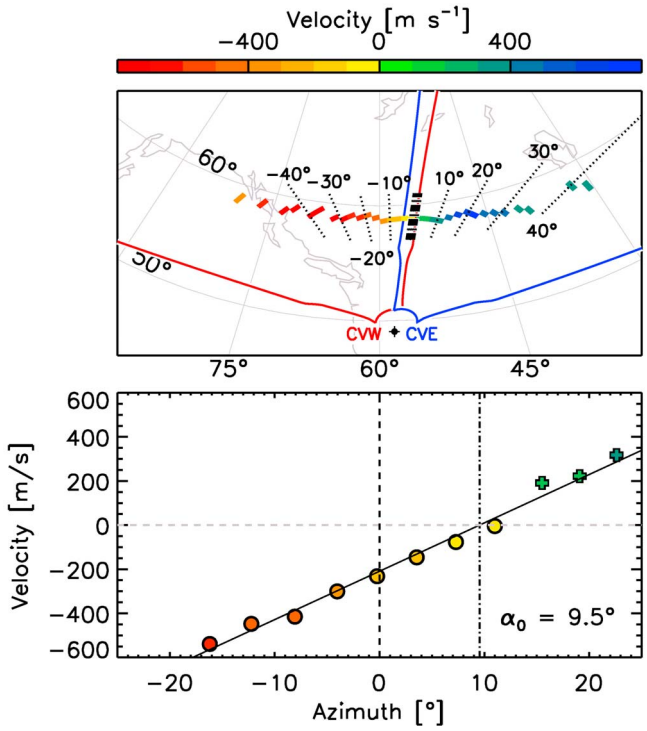

Figure 6. (top) In magnetic coordinates, the highest westward LOS velocities selected at each beam of the CVW and CVE radar. The red and blue lines give the FOV of the CVW and CVE radar, respectively. The dash-dotted line in the overlap of the two FOV gives the azimuth angle α_0 at which the velocity flow is perpendicular to the radar look direction. The dotted lines give look directions relative to α_0 in 10° increments. (bottom) The same velocity data as in Figure 6 (top), but now plotted against the beam azimuth angle. Data from CVW are plotted as circles, data from CVE are shown as crosses. The line is a linear fit to the velocities with $-20° \le \alpha \le 20°$. The azimuth at which the fit is equal to 0 (at $\alpha = \alpha_0$) is marked by a vertical dash-dotted line.

American sector where the velocities measured by the CVW radar exceed 1000 m/s; but enhanced velocities can still be observed over the eastern part in the data from WAL at about 100 m/s. At 0840 UT the flow inside the channel is in the opposite direction from generally eastward flows observed at higher latitudes ($\Lambda > 60°$), as is best observed in data from CVW and BKS.

[20] Between 0830 and 0850 the POES-18 satellite crossed over central northern America, measuring the downgoing electron flux, which is generally highest inside the auroral oval due to precipitating electrons. It can then be seen from the POES-18 data shown in Figure 5 (top) that the auroral oval in the local time sector of the satellite crossing was located about 2–3° poleward of the observed flow channel. High westward velocities inside a relatively narrow channel observed equatorward of the auroral oval are then convincing evidence that the feature observed by the mid-latitude radars was indeed a SAPS [*Foster and Burke*, 2002; *Oksavik et al.*, 2006].

[21] Determining the geomagnetic location of radar backscatter from the beam direction and the travel time of the HF signal between the radar and the scatter location in a spatially and temporally varying ionosphere is not a trivial task. The radar velocity data shown in Figure 5 was mapped using the standard SuperDARN virtual height model; *Chisham et al.* [2008] presented a more sophisticated model for mapping radar scatter with greater accuracy than the standard model. At all radars used in this study the range, i.e., the distance traveled by the HF signal from the radar to the scatter location inside the SAPS was about 1500 km. According to the study by *Chisham et al.* [2008] using the standard model at these ranges introduces an error in that the standard model locates the scatter about 100 km equatorward of that location determined when using the improved model. This roughly translates to a latitudinal error of about 1°. Even though the standard mapping places the scatter location about 1° equatorward of its more likely position, we can still assume with confidence that the SAPS location is equatorward of the equatorward boundary of the main auroral oval as identified by the electron precipitation.

[22] It should be noted that careful analysis of Doppler velocity data from the Hokkaido radar, which is located in northern Japan and looking toward Alaska - the Hokkaido radar FOV is shown in the top left corner of Figure 1 in orange - shows traces of high-velocity westward flows over eastern Siberia, i.e., about 3 hours MLT west of the CVW observations, indicating the large spatial extent of this particular SAPS. The quality of the backscatter from these flows measured by the Hokkaido radar, however, was poor such that it cannot be used for quantitative analysis.

3. Velocity Analysis

[23] In order to compare velocity measurements from inside the SAPS channel made by different radars along different beams in a meaningful sense, we need to find the flow direction of the SAPS. There are at least two ways of combining LOS velocity data from different look directions to reconstruct the original 2D flow. One involves combining LOS measurements made in a common volume by two radars [*Hanuise et al.*, 1993]. During the event period discussed in this paper common volume velocity measurements by two radars were unfortunately rare, so in order to maximize the coverage of the velocity solution, we use a different technique, which is similar to L-shell fitting [*Villain et al.*, 1987; *Ruohoniemi et al.*, 1989]. If we assume the flow is constant in magnitude and direction across some portion of the FOV of one or several radars, the flow direction is perpendicular to that look direction across which the LOS velocity changes sign. By identifying the azimuth α_0 across which the LOS measurements made by two adjacent radars (CVW & CVE, FHW & FHE, BKS & WAL) change sign we find the local flow direction for each radar pair at every time step. We can then choose beams symmetric to that flow direction. Under the above assumption the measured LOS velocities along beams symmetric to α_0 are then equal. If, however, the LOS velocities in symmetric beams are not equal, we gain information about the longitudinal variation of the flow velocity inside the SAPS channel.

[24] Figure 6 illustrates how the flow direction is identified using the method described above. First, from each beam sounding made by all radars we select the maximum LOS velocity with a westward sense, in the same way as is shown in the second panel of Figure 4. In Figure 6 (top), we

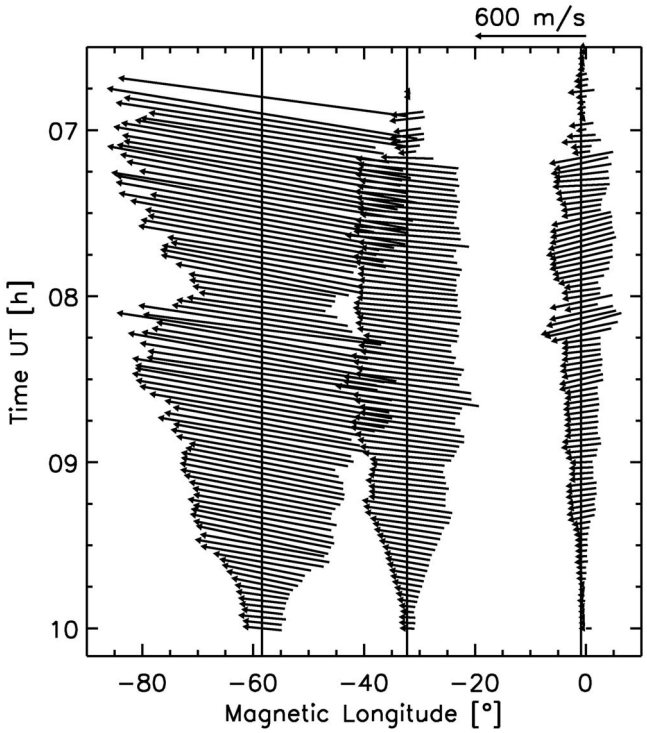

Figure 7. Vector representation of the average large-scale SAPS flow direction and the inferred SAPS speed identified by the three radar pairs. Time runs along the *y* axis, increasing toward to bottom.

show the locations and values of the maximum velocities for each beam of the Christmas Valley radar pair at 0840 UT. In Figure 6 (bottom) we show the same velocities, now plotted against beam azimuth, i.e. the look direction of each beam relative to magnetic North. Measurements from CVW are shown as circles, velocities measured by CVE are shown as crosses. It can be seen from Figure 6 (bottom), that at $\alpha = 0°$ (the beam looking due magnetic North marked by a vertical dashed line) the velocity is not zero, indicating a significant north-south component of the flow inside the SAPS channel.

[25] To identify that azimuth α_0 where the observed LOS velocity was zero, we least squares fit a function to the LOS velocities. In full L-shell fitting this function is a superposition of a zonal velocity component, which varies as a cosine of the beam azimuth, and a meridional velocity component, represented by a sine [*Ruohoniemi et al.*, 1989]. Because here we are not fitting across the entire FOVs but rather are just interested in that location where the LOS velocity as a function of azimuth goes through zero, we limit our fit to azimuths between $-20° \leq \alpha \leq 20°$ and fit a linear trend to all LOS velocities in this range. For the Christmas Valley radar pair at 0840 UT the fit to these LOS velocity values is shown as a solid black line in Figure 6 (bottom). In that figure we also show the resulting α_0 as a vertical dash-dotted line.

[26] Using the above method we can identify α_0 and hence the local flow direction for the Christmas Valley, Fort Hays and Virginia radar pair for each radar scan at 2-minute time resolution. Having identified the flow direction we can select beams symmetric to it, i.e. those beams from different radars whose azimuth is the same relative to the flow direction. By selecting such symmetric beams we effectively eliminate from the measurements the influence due to the angle between the look direction of the beams and the local flow direction. Thus, if velocity measurements from symmetric beams show systematic differences along the flow channel, these must be due to actual geophysical variations in the flow of the SAPS. Furthermore, by selecting beams with a known angle α_L with respect to α_0, we can infer the total velocity inside the SAPS by dividing the measured LOS velocities by sin α_L. We find that an angle of $\alpha_L = 20°$ yields good results and all ionospheric velocities presented in the following plots are what we call "inferred SAPS velocities", i.e. velocity measurements by the SuperDARN radars which have been corrected to account for the local flow direction and the look direction of each radar beam.

[27] In Figure 7 we show the local flow direction and the inferred SAPS speed identified in data from the three radar pairs as vectors. The *x* axis gives magnetic longitude; the vectors are centered on the longitude of the average radar location (compare Table 1). Time runs along the *y* axis, it increases toward the bottom of the plot. The length of each flow vector is proportional to the inferred SAPS speed; the speed scale is given above the panel. The angle each flow vector makes with the vertical axis gives its azimuth relative to magnetic North, i.e. $\alpha_0 - 90°$. Figure 7 shows that the flow direction is very stable during the course of the event. The radar pairs are roughly equally spaced in longitude, however the observed velocity is halved from the Oregon to the Kansas radar pair, and again halved from the Kansas to the Virginia radar pair. This indicates an exponential dependence of the velocities on magnetic longitude. Furthermore, the flow channel arcs with longitude, in the East it has a southward component whereas in the West, it shows significant northward flow.

[28] Now that we have eliminated the effect due to the variability of the angle between the radar look direction and the local flow direction from the observed velocity measurements, we can investigate how the velocity inside the SAPS channel varied as a function of MLT and UT. For two hours of data we plot the inferred SAPS velocity on a logarithmic scale against the instantaneous magnetic local time at which the measurement was made (see Figure 8). Different symbols correspond to measurements by different radars, according to the legend in the top right corner. The measurements are colored according to the time at which they were observed; see the color bar on the right.

[29] Figure 8 shows that the instantaneous variation with MLT of the SAPS velocity $v_{\mathrm{saps},t}$ is well approximated by an exponential function, with the highest velocities observed in the western-most parts of the radar FOVs:

$$v_{\mathrm{saps},t}(m) = v_{0,t} e^{-\lambda_t m} \tag{1}$$

The parameters $v_{0,t}$ and λ_t in (1) are dependent on time *t*, which has been expressed by adding the subscript *t*; *m* gives the magnetic local time, λ_t is the slope of the exponential MLT dependence, and $v_{0,t}$ represents the intercept with the ordinate at 00 MLT. Figure 8 also shows that for the first 1 1/2 hours (0800–0930 UT) λ_t as well as $v_{0,t}$ remain fairly constant. During the last half hour of the event (0930–1000 UT) the velocities decreased such that $v_{0,t}$ dropped to lower values while λ_t remained essentially unchanged.

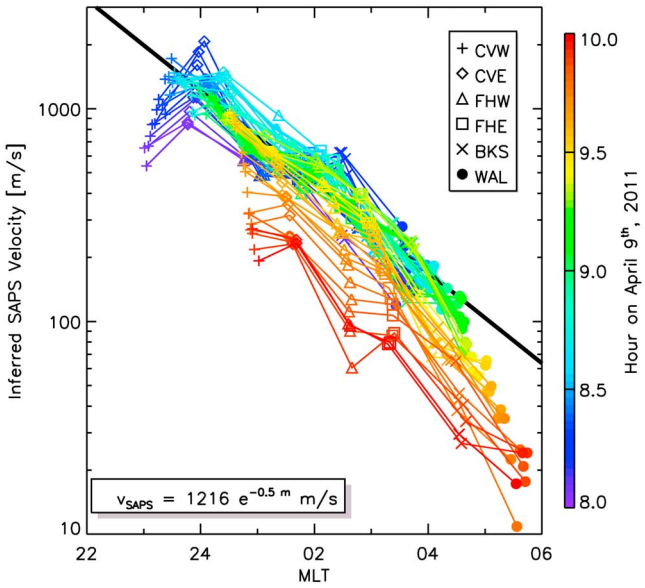

Figure 8. Longitudinal variation of the inferred SAPS velocity measured by all six radars. The black line shows an exponential function whose amplitude and decay factor were determined from exponential fits to velocity profiles at each time step between 0800 and 0930 UT. The functional form of the black line is given in the bottom left corner of the plot. See text for further detail.

[30] For each magnetic local time velocity profile measured between 0800 and 0930 UT which contains more than three valid points, we fit an exponential function like (1) to the inferred velocities. We then average the fit parameters λ_t and $v_{0,t}$ between 0800 and 0930 UT to obtain an average value for the velocity and decay parameter, v_0 and λ, respectively. According to our analysis the flow velocity inside the SAPS channel at 00 MLT during the event studied in this paper was around 1200 m/s. The velocity decayed exponentially with longitude toward dawn, the e-folding spatial scale of the longitudinal velocity variation was 2 hours MLT. An exponential function with these parameters is shown as a thick black line in Figure 8, its functional form is given in the lower left corner of the plot.

4. Discussion

[31] The SuperDARN observations of the SAPS event presented in this paper cover about six hours of magnetic local time. Using information about the flow direction as described in the previous section, we are able to evaluate the longitudinal variation of the flow speed inside the SAPS, the "inferred SAPS velocity". The linear variation with MLT reported from statistical studies by *Foster and Vo* [2002] and *Erickson et al.* [2011] was not seen in this study of instantaneous velocities, rather, we find that the change in velocity with local time is best approximated by an exponential function. Using such MLT dependence we find that the velocity inside this particular SAPS was about 1200 m/s at 00 MLT and had a spatial e-folding scale of 2 hours of MLT.

[32] As outlined in the introduction, the current understanding of the formation of SAPS links its occurrence to the presence of field-aligned currents, which in turn are driven by pressure gradients in the ring current [e.g., *Toffoletto et al.*, 2003]. If one, to first order, assumes a linear relationship between the SAPS velocity and the pressure gradient in the ring current, our results suggest that an exponential variation of the velocity with MLT implies the same dependence of the pressure gradient in the magnetosphere. To pursue this point we trace the locations of the maximum westward velocities observed in symmetric beams into the magnetospheric equatorial plane using the Tsyganenko-96 magnetic field model [*Tsyganenko*, 1995]. Note that we are tracing the ionospheric locations of scatter points within the SAPS, we are not mapping measured vector electric fields along magnetic field lines into the equatorial plane. The latter would require the usage of scaling factors similar to those described by *Mozer* [1970] which would change the magnitude and direction of the field in the equatorial plane. The resulting positions at 20 minute intervals between 0700 and 1000 UT are shown in the X-Y GSM plane in Figure 9. In all panels of Figure 9 the Sun is to the left and dashed lines mark geocentric distances at 2, 4 and 6 Earth radii (R_e). The locations have been color-coded by the observed ionospheric LOS velocity. As the radars rotate with Earth, the locations trace an arc that stretches from about 4.2 R_e in the

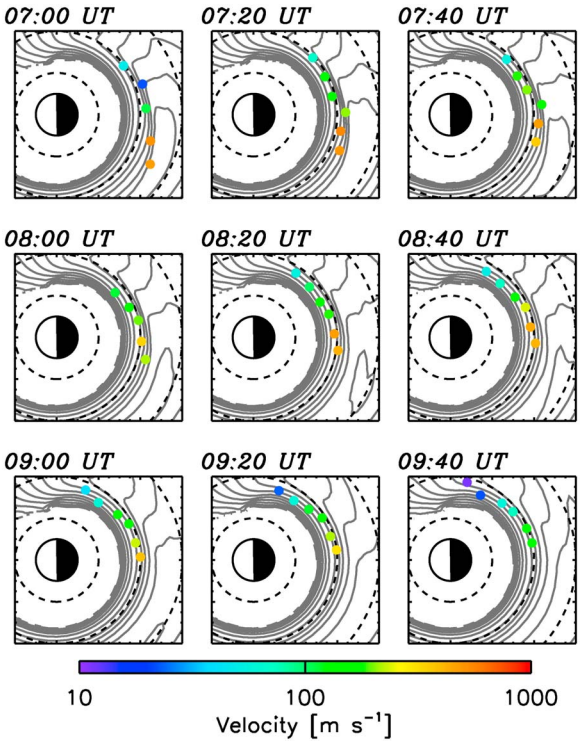

Figure 9. In each panel we show the magnetospheric equatorial plane; the Sun is located to the left. The dots mark the locations of the maximum westward velocity observed along each beam traced into the equatorial magnetosphere. For the tracing we used the T96 model with appropriate solar wind input parameters (pdyn = 1.3 nPa, Dst = −40 nT, By = −1 nT, and Bz IMF = −3 nT). The gray lines are contours of the logarithm of total plasma pressure predicted by the RCM inner-magnetosphere model which was run for the same solar wind parameters. The dashed lines are located at 2, 4, and 6 R_e.

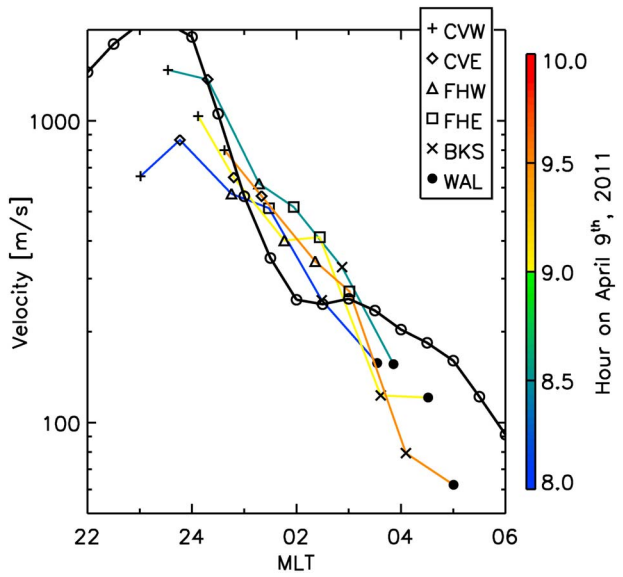

Figure 10. Comparison between modeled and inferred SAPS velocities. The model values are shown as a solid black line and open circles. The inferred velocity profiles at different times are shown as solid lines which have been color-coded according to the color bar on the right. Different symbols marking the inferred velocities indicate measurements by different radars, as given by the legend in the top right corner.

pre-midnight sector to about 3.8 R_e at 06 MLT. This variation in geocentric distance, or equivalently magnetic latitude, of the SAPS channel with MLT is well known [*Erickson et al.*, 2011].

[33] Models of the inner magnetosphere such as the Rice-Convection Model (RCM) are capable of predicting the plasma pressure in the inner magnetosphere and the flow velocities in the ionosphere associated with pressure gradients. We ran the RCM for the prevailing conditions on April 9 2010 and indeed, the model showed the formation of a SAPS at the precise time with similar magnitude and location as it was observed by the radars. In Figure 9 we show the contours of the logarithm of the total plasma pressure as predicted by the model. The total plasma pressure as predicted by the RCM shows a maximum in the pre-midnight sector around 4.5 R_e. Figure 9 shows that the trace locations of the ionospheric maximum velocities are as expected located in the vicinity of strong gradients of the plasma pressure and are during all times approximately spaced by equal amounts of contour levels. Therefore, we feel that the exponential trend in plasma pressure generally holds and can explain the observed longitudinal variation of the velocities in SAPS.

[34] *Zheng et al.* [2008] combined a comprehensive ring current model with a model of ionospheric conductances which included an artificial density trough region. They were able to show how the FACs produced by the pressure gradients in the plasma sheet caused the formation of a SAPS channel in the ionosphere. As *Zheng et al.* [2008] showed, the location of the SAPS formation is determined by the location of the density trough in the ionosphere; so much so that under identical driving conditions the model does not produce a SAPS if no local decrease in ionospheric density is included.

[35] From the model run by *Zheng et al.* [2008] we extract maximum ionospheric velocities within the modeled SAPS as a function of MLT. We then plot these velocity values as a solid black line in Figure 10; each individual datum is marked by an open circle. Superimposed on these model values we show the inferred SAPS velocities from SuperDARN observations at different times, where the time of the measurement is color-coded according to the color bar on the right. It can be seen that the agreement both in magnitude and variation with MLT between the modeled and measured velocity values is very good. This indicates that the model presented by *Zheng et al.* [2008] is capable of accurately predicting the ionospheric flows created by FACs which are driven by pressure gradients in the ring current. Furthermore, it also indicates that the velocity in a SAPS event decays exponentially with MLT away from midnight.

[36] Apart from the large-scale variation of the velocities with magnetic local time, which according to Figure 8 was fairly constant over the course of this event, the radar observations also showed considerable temporal variations in the SAPS, as evident from varying flow vector length at each radar location in Figure 7. These temporal variations are well correlated between measurements from all radars (correlation coefficient R $\sim$ 80%), but poorly correlated with activity parameters such as AL, AU, or Sym-H. This is probably due to the fact that these activity indices are derived globally, whereas the velocity measurements were made within a smaller region. The best correlation (R $\sim$ 70%) is observed for Asym-H. This is not too surprising as the Asym-H index is a measure for the asymmetric ring current that is the driver of the Region-2 FACs which in turn cause the large electric fields and hence flows in the ionosphere. However, the good correlation between Asym-H and the SAPS velocity is more due to the overall agreement of the two time series during this event (compare Figure 4); individual decreases and increases in the flow velocity were not matched by according variations in the Asym-H index.

[37] Temporal changes in the FAC strength are also possible causes for variations in the SAPS velocity; as these are quite localized, subtle changes [*Zheng et al.*, 2008], the global Asym-H index might not be able to detect them. Instead, one should look for localized measurements of FACs, such as the newly available AMPERE dataset (B. J. Anderson et al., AMPERE: Overview and initial results, manuscript in preparation, 2012). Another possibility is to relate the SAPS velocity with signatures of electron precipitation. Initial analysis of ground-based all-sky imager data from stations located in Canada as part of the THEMIS mission indicate good potential to investigate this relationship. Such an analysis is left for future work.

[38] Another factor that conceivably influences the velocities observed in the midlatitude ionosphere is the depth and width of the density trough. As the plasma pressure gradient in the magnetosphere drives field-aligned currents (FACs) into the ionosphere, these must close via Pedersen currents. If the FACs must close across a region where the conductance is low, large electric fields develop which manifest themselves as strong flows. In fact, *Zheng et al.* [2008] also show that for identical magnetospheric conditions SAPS only occur if such a region of low

ionospheric conductance exists. As outlined in the introduction, strong electric fields cause further reduction of the conductivity, leading to positive feedback. In Figure 5 we showed simultaneous GPS TEC measurements co-located with the velocity observations inside the SAPS channel. These show that the SAPS was - as expected - located in a region of low TEC, which is indicative of the trough where ionospheric conductivity is known to be low. Initial analysis of the TEC data suggests that the width and depth of the low-conductance region in the ionosphere was relatively stable during this event. A detailed analysis of the TEC measurements, however, is beyond the scope of this study and will be presented in a future paper.

5. Conclusions

[39] On 09 April 2011 a SAPS was observed by six mid-latitude SuperDARN radars. In this study we have presented instantaneous velocity measurements from within the SAPS channel continuously covering more than six hours of magnetic local time for three hours of universal time. Assuming constant flow direction and magnitude within the SAPS over some part of the FOV of the three radar pairs we reconstruct 2D ionospheric flows inside the SAPS channel. Our analysis shows that during this event the flow direction was very stable, however the flow speed showed significant temporal variations. The flow within the SAPS is predominantly westward. Toward earlier MLTs the flow acquires a significant southward component while toward later MLTs it has a northward component.

[40] From examination of the large-scale distribution of the velocities associated with this SAPS event we conclude that the velocity magnitude decreases exponentially with MLT in the morning sector. Using modeled plasma pressure values at conjugate points in the magnetospheric equatorial plane we show that the exponential decrease in velocity is matched by an exponential decrease in plasma pressure. As plasma pressure gradients drive field-aligned currents, which in turn are believed to cause SAPS, we tentatively conclude that the pressure distribution in the magnetospheric equatorial plane partly determines the ionospheric velocities.

[41] These conclusions are supported by the very good agreement between the ionospheric velocities observed by the SuperDARN radars and the results of a ring current model which includes the calculation of the associated FACs and influences by a ionospheric region of low conductance.

[42] Simultaneous measurements of the TEC using GPS receivers are presented and show that the SAPS was located, as expected, in a region of low ionospheric density. Further studies of the TEC values will show to what extent variability in the ionospheric conductivity influences the flow velocities observed inside the SAPS.

[43] The analysis presented in this paper clearly shows the impressive possibilities the new chain of SuperDARN radars offers for studying midlatitude phenomena such as SAPS.

[44] **Acknowledgments.** The AU, AL, Sym-H, and Asym-H index data were downloaded from the World Data Centre for Geomagnetism, Kyoto. The Kp index data were downloaded from the GFZ German Research Centre for Geosciences, Potsdam. POES-18 data were accessed through the National Geophysical Data Center (NGDC) of the National Oceanic and Atmospheric Administration (NOAA), Boulder. The TEC data were downloaded through the Madrigal database at Haystack Observatory. LBNC acknowledges funding for his GEM postdoctoral fellowship from the National Science Foundation under grant ATM-0924919. LBNC also acknowledges funding from the Deutsches Zentrum für Luft- und Raumfahrt under grants 50OC1102 and 50OC1001. JBHB, JMR, and RAG acknowledge the support of the National Science Foundation under grant ATM-0838219 and ATM-0946900. SGS acknowledges the support of the National Science Foundation under grant ATM-0838356. ERT acknowledges the support of the National Science Foundation under grant ATM-0838142. WAB acknowledges the support of the National Science Foundation under grant ATM-0838270.

[45] Robert Lysak thanks Kjellmar Oksavik and another reviewer for their assistance in evaluating this paper.

References

Alfvén, H. (1955), On the electric field theory of magnetic storms and aurorae, *Tellus*, *7*, 50–64.

Alfvén, H. (1958), On the theory of magnetic storms and aurorae, *Tellus*, *10*, 105–108.

Anderson, B. J. (1993), Statistical studies of Pc 3–5 pulsations and their relevance for possible source mechanisms of ULF waves, *Ann. Geophys.*, *11*, 128–143.

Anderson, P. C., D. L. Carpenter, K. Tsuruda, T. Mukai, and F. J. Rich (2001), Multisatellite observations of rapid subauroral ion drifts (SAID), *J. Geophys. Res.*, *106*, 29,585–29,600, doi:10.1029/2001JA000128.

Baker, K. B., and S. Wing (1989), A new magnetic coordinate system for conjugate studies at high latitudes, *J. Geophys. Res.*, *94*, 9139–9143, doi:10.1029/JA094iA07p09139.

Banks, P. M., and F. Yasuhara (1978), Electric fields and conductivity in the nighttime E-region: A new magnetosphere-ionosphere-atmosphere coupling effect, *Geophys. Res. Lett.*, *5*, 1047–1050, doi:10.1029/GL005i012p01047.

Chisham, G., et al. (2007), A decade of the Super Dual Auroral Radar Network (SuperDARN): Scientific achievements, new techniques and future directions, *Surv. Geophys.*, *28*, 33–109, doi:10.1007/s10712-007-9017-8.

Chisham, G., T. K. Yeoman, and G. J. Sofko (2008), Mapping ionospheric backscatter measured by the SuperDARN HF radars—Part 1: A new empirical virtual height model, *Ann. Geophys.*, *26*, 823–841.

Coster, A. J., M. J. Colerico, J. C. Foster, W. Rideout, and F. Rich (2007), Longitude sector comparisons of storm enhanced density, *Geophys. Res. Lett.*, *34*, L18105, doi:10.1029/2007GL030682.

Erickson, P. J., F. Beroz, and M. Z. Miskin (2011), Statistical characterization of the American sector subauroral polarization stream using incoherent scatter radar, *J. Geophys. Res.*, *116*, A00J21, doi:10.1029/2010JA015738.

Evans, D. S., and M. S. Greer (2000), Polar orbiting environmental satellite space environment monitor 2: Instrument description and archive data documentation, *Tech. Memo., OAR SEC-93*, NOAA, Boulder, Colo.

Foster, J. C., and W. J. Burke (2002), SAPS: A new categorization for sub-auroral electric fields, *Eos Trans. AGU*, *83*, 393–394, doi:10.1029/2002EO000289.

Foster, J. C., and H. B. Vo (2002), Average characteristics and activity dependence of the subauroral polarization stream, *J. Geophys. Res.*, *107*(A12), 1475, doi:10.1029/2002JA009409.

Galperin, Y. I. (2002), Polarization jet: Characteristics and a model, *Ann. Geophys.*, *20*, 391–404, doi:10.5194/angeo-20-391-2002.

Galperin, Y. I., Y. N. Ponomarov, and A. G. Zosinova (1973), Direct measurements of ion drift velocity in the upper atmosphere during a magnetic storm, *Kosm. Issled.*, *11*, 273–283.

Greenwald, R. A., et al. (1995), Darn/Superdarn: A global view of the dynamics of high-latitude convection, *Space Sci. Rev.*, *71*, 761–796, doi:10.1007/BF00751350.

Greenwald, R. A., K. Oksavik, P. J. Erickson, F. D. Lind, J. M. Ruohoniemi, J. B. H. Baker, and J. W. Gjerloev (2006), Identification of the temperature gradient instability as the source of decameter-scale ionospheric irregularities on plasmapause field lines, *Geophys. Res. Lett.*, *33*, L18105, doi:10.1029/2006GL026581.

Hall, G. E., J. W. MacDougall, D. R. Moorcroft, J.-P. St.-Maurice, A. H. Manson, and C. E. Meek (1997), Super Dual Auroral Radar Network observations of meteor echoes, *J. Geophys. Res.*, *102*, 14,603–14,614, doi:10.1029/97JA00517.

Hanuise, C., C. Senior, J.-C. Cerisier, J.-P. Villain, R. A. Greenwald, J. M. Ruohoniemi, and K. B. Baker (1993), Instantaneous mapping of high-latitude convection with coherent HF radars, *J. Geophys. Res.*, *98*, 17,387–17,400, doi:10.1029/93JA00813.

Holzworth, R. H., and C.-I. Meng (1975), Mathematical representation of the auroral oval, *Geophys. Res. Lett.*, *2*, 377–380.

Kavanagh, L. D., Jr., J. W. Freeman Jr., and A. J. Chen (1968), Plasma flow in the magnetosphere, *J. Geophys. Res.*, *73*(17), 5511–5519, doi:10.1029/JA073i017p05511.

Kennel, C. F. (1969), Consequences of a magnetospheric plasma, *Rev. Geophys.*, *7*, 379–419, doi:10.1029/RG007i001p00379.

King, J., and N. Papitashvili (2006), One min and 5-min solar wind data sets at the Earth's bow shock nose, NASA Goddard Space Flight Cent., Greenbelt, Md.

Makarevich, R. A., A. C. Kellerman, Y. V. Bogdanova, and A. V. Koustov (2009), Time evolution of the subauroral electric fields: A case study during a sequence of two substorms, *J. Geophys. Res.*, *114*, A04312, doi:10.1029/2008JA013944.

Mozer, F. S. (1970), Electric field mapping in the ionosphere at the equatorial plane, *Planet. Space Sci.*, *18*, 259, doi:10.1016/0032-0633(70)90161-3.

Oksavik, K., R. A. Greenwald, J. M. Ruohoniemi, M. R. Hairston, L. J. Paxton, J. B. H. Baker, J. W. Gjerloev, and R. J. Barnes (2006), First observations of the temporal/spatial variation of the sub-auroral polarization stream from the SuperDARN Wallops HF radar, *Geophys. Res. Lett.*, *33*, L12104, doi:10.1029/2006GL026256.

Ribeiro, A. J., J. M. Ruohoniemi, J. B. H. Baker, L. B. N. Clausen, S. de Larquier, and R. A. Greenwald (2011), A new approach for identifying ionospheric backscatter in midlatitude SuperDARN HF radar observations, *Radio Sci.*, *46*, RS4011, doi:10.1029/2011RS004676.

Rideout, W., and A. Coster (2006), Automated GPS processing for global total electron content data, *GPS Solut.*, *10*, 219–228, doi:10.1007/s10291-006-0029-5.

Ruohoniemi, J. M., and R. A. Greenwald (1996), Statistical patterns of high-latitude convection obtained from Goose Bay HF radar observations, *J. Geophys. Res.*, *101*, 21,743–21,764, doi:10.1029/96JA01584.

Ruohoniemi, J. M., R. A. Greenwald, K. B. Baker, J. P. Villain, and M. A. McCready (1987), Drift motions of small-scale irregularities in the high-latitude F region: An experimental comparison with plasma drift motions, *J. Geophys. Res.*, *92*, 4553–4564, doi:10.1029/JA092iA05p04553.

Ruohoniemi, J. M., R. A. Greenwald, K. B. Baker, J.-P. Villain, and C. Hanuise (1989), Mapping high-latitude plasma convection with coherent HF radars, *J. Geophys. Res.*, *94*, 13,463–13,477, doi:10.1029/JA094iA10p13463.

Schunk, R. W., P. M. Banks, and W. J. Raitt (1976), Effects of electric fields and other processes upon the nighttime high-latitude F layer, *J. Geophys. Res.*, *81*, 3271–3282, doi:10.1029/JA081i019p03271.

Smiddy, M., R. Sagalyn, B. Shuman, M. C. Kelley, W. Burke, F. Rich, R. Hays, and S. Lai (1977), Intense poleward-directed electric fields near the ionospheric projection of the plasmapause, *Geophys. Res. Lett.*, *4*, 543–546, doi:10.1029/GL004i011p00543.

Southwood, D. J., and R. A. Wolf (1978), An assessment of the role of precipitation in magnetospheric convection, *J. Geophys. Res.*, *83*, 5227–5232, doi:10.1029/JA083iA11p05227.

Spiro, R. W., R. A. Heelis, and W. B. Hanson (1979), Rapid subauroral ion drifts observed by Atmosphere Explorer C, *Geophys. Res. Lett.*, *6*, 657–660, doi:10.1029/GL006i008p00657.

Toffoletto, F., S. Sazykin, R. Spiro, and R. Wolf (2003), Inner magnetospheric modeling with the Rice Convection Model, *Space Sci. Rev.*, *107*, 175–196, doi:10.1023/A:1025532008047.

Tsyganenko, N. A. (1995), Modeling the Earth's magnetospheric magnetic field confined within a realistic magnetopause, *J. Geophys. Res.*, *100*(A9), 5599–5612.

Villain, J. P., R. A. Greenwald, K. B. Baker, and J. M. Ruohoniemi (1987), HF radar observations of E region plasma irregularities produced by oblique electron streaming, *J. Geophys. Res.*, *92*, 12,327–12,342, doi:10.1029/JA092iA11p12327.

Wolf, R. A., R. W. Spiro, S. Sazykin, and F. R. Toffoletto (2007), How the Earth's inner magnetosphere works: An evolving picture, *J. Atmos. Terr. Phys.*, *69*(3), 288–302, doi:10.1016/j.jastp.2006.07.026.

Yeh, H.-C., J. C. Foster, F. J. Rich, and W. Swider (1991), Storm time electric field penetration observed at mid-latitude, *J. Geophys. Res.*, *96*, 5707–5721, doi:10.1029/90JA02751.

Zheng, Y., P. C. Brandt, A. T. Y. Lui, and M.-C. Fok (2008), On ionospheric strough conductance and subauroral polarization streams: Simulation results, *J. Geophys. Res.*, *113*, A04209, doi:10.1029/2007JA012532.